Templates of expected measurement uncertainties for prompt fission neutron spectra

Denise Neudecker, Matthew Devlin, Robert C Haight, Keegan J Kelly, Paola Marini, Allan D Carlson, Julien Taieb, Morgan C White

Templates of Expected Measurement Uncertainties for Prompt Fission Neutron Spectra

D. Neudecker[a]*, M. Devlin[a], R.C. Haight[a], K.J. Kelly[a], P. Marini[b,c], A.D. Carlson[d], J. Taieb[b,e], M.C. White[a]
[a]Los Alamos National Laboratory, P.O. Box 1663, MS-P365, Los Alamos, New Mexico 87545, USA,
[b] CEA, DAM, DIF, F-91297 Arpajon, France,
[c] Univ. Bordeaux, LP2I, UMR5797, CNRS, F-33170, Gradignan, France,
[d]National Institute of Standards and Technology, Gaithersburg, MD 20899-8463, USA,
[e] Université Paris-Saclay, CEA, LMCE, 91680 Bruyères-le-Châtel, France

August 8, 2023

Abstract

In this paper, we provide templates of uncertainty sources expected to appear for three measurement types of prompt fission neutron spectra (PFNS): (1) Shape measurements, (2) clean-ratio shape, that is the monitor PFNS are measured in nearly exactly the same surrounding as the PFNS of interest, and (3) indirect ratios, where the detector efficiency is backed out from PFNS monitor measurements. Information is also listed that is needed to faithfully include PFNS into nuclear data evaluations to guide experimenters how to best report data and metadata for their measurements. These templates also suggest a typical range of pertinent uncertainty values and their correlations in case realistic uncertainties cannot be estimated from information on the measurement itself. The templates were based on a literature review, information found in EXFOR for ^{252}Cf, ^{235,238}U, and ^{239}Pu PFNS, and enhanced by expertise from experimenters contributing to these PFNS templates.

LA-UR-22-32111

1 Introduction

A prompt-fission neutron spectrum (PFNS) describes the energy distribution of neutrons emitted from fission fragments from an actinide in a time window promptly after fission and before the onset of beta decay [1]. The fission reaction can be induced by neutrons, as *e.g.*, for neutron-induced ^{235}U(n,f) PFNS, or be spontaneous, as, *e.g.*, for the case of the PFNS standard, namely the ^{252}Cf spontaneous fission spectrum [2–4] that is shown in Fig. 1. A PFNS gives a probability distribution of neutrons to be emitted at a specific outgoing-neutron energy, $E_{\rm out}$. Thus, the evaluated data are normalized such that the integral over the PFNS gives unity [5]. The maximum of this distribution is usually in the low-MeV range—dependent on the isotope at hand. At higher $E_{\rm out}$, the spectrum falls off, such that there can be a few orders of magnitude difference in the PFNS between its peak and, *e.g.*, at $E_{\rm out} = 10$ MeV (see left-hand side of Fig. 1). It is very difficult to detect neutrons of the PFNS to high statistical precision for $E_{\rm out} > 10$ MeV due to the paucity of emitted neutrons in this energy range and cosmic backgrounds. Special background-reduced environments must be sought for measurements at $E_{\rm out} > 20$ MeV (a former lead mine under a 1000 m mountain was used, for instance, for Ref. [6]).

*E-mail of corresponding author: dneudecker@lanl.gov; Phone-number: +1-(505)-665 3354

It is equally difficult to precisely measure the PFNS at low E_{out}, *e.g.*, below 10 keV in even favorable experimental conditions, because of the prevalence of background and multiple-scattered neutrons that can be larger in numbers than the desired prompt-fission neutrons. These limitation in measuring the PFNS at high and low E_{out} can be observed by the higher uncertainties and scatter among data points in the right-hand side of Fig. 1. In these energy ranges, below 10 keV and above 10 MeV, nuclear model forms or integral information help to define evaluated PFNS, even if sufficient experimental data are available for other E_{out} ranges.

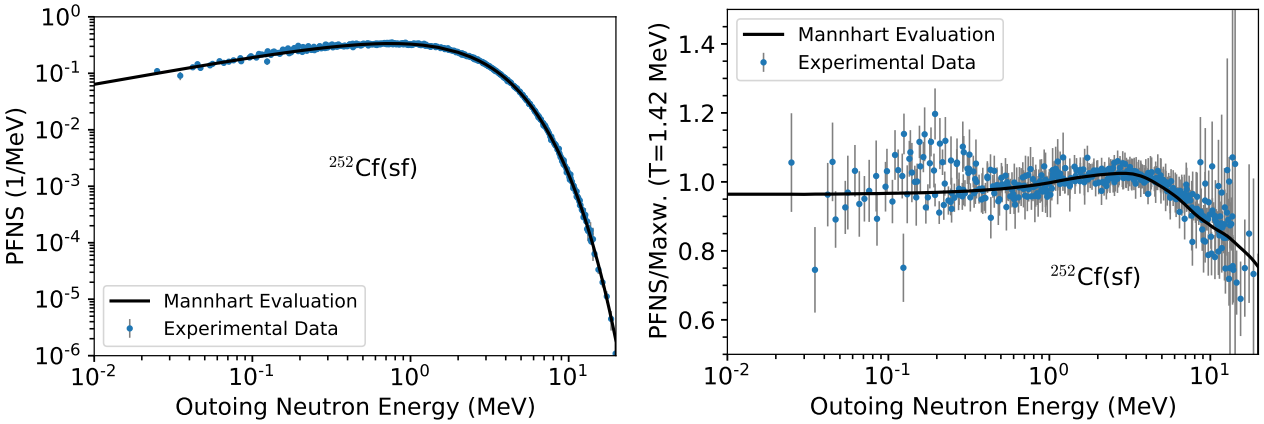

(a) The PFNS in units of (1/MeV).

(b) The PFNS as a ratio to a Maxwellian function.

Figure 1: The evaluated ^{252}Cf spontaneous fission spectrum by Mannhart [2, 3] is compared to the experimental data used for that evaluation and as shown in Figs. 1–10 of Refs. [2].

Below, a template of expected measurement uncertainties is provided for PFNS. These templates were developed for obtaining PFNS via the time-of-flight (TOF) technique to determine E_{out} of the PFNS as this is the most frequently employed technique. If other techniques are used (like measuring the E_{out} directly, using n-p scattering and a proton recoil spectrometer) recourse should be taken to other templates that describe these techniques.

The template described here was established based on (a) the uncertainty procedure developed within the IAEA Coordinated Research Project on PFNS documented in Chapter III.M of Ref. [1], (b) the detailed uncertainty analysis [7–9] of several ^{235,238}U and ^{239}Pu PFNS experimental data using their respective literature [10–34] and EXFOR entries [35], as well as (c) uncertainty studies undertaken by the Chi-Nu team as part of their measurement campaign [13,36–41]. After the initial establishment of the templates, a sub-set of the authors reviewed ^{252}Cf PFNS measurements; some of the knowledge, gained from Refs. [6, 42–44], was added to this manuscript.

2 Measurement Types

PFNS are typically experimentally determined from time-of-flight (TOF) measurements of outgoing neutrons.. PFNS can be measured for spontaneous fission or as a function of incident-neutron energy, E_{inc}. In the latter case, one can use mono-energetic neutron beams, where E_{inc} is well-defined, see, *e.g.*, Ref. [16, 45]. PFNS can also be measured with white-neutron sources. In this case, the TOF technique is also applied to measure E_{inc} as, for instance, in Ref. [38, 46].

The techniques for measuring a PFNS are distinguished according to how the neutron detector efficiency, ε, was derived. This specific partition was chosen because different uncertainty-quantification methods have to be applied to estimate total PFNS covariances depending on how ε was determined. This is described in detail in the appendix of Ref. [47].

2.1 PFNS Shape Measurements

In a PFNS shape measurement[1] (illustrated schematically in the upper panel of Fig. 2), ε is determined directly. It is either measured by a non-PFNS experiment or simulated/ calculated. For instance, Knitter [17] measured ε relative to neutron-production cross sections, while Staples *et al.* [45] obtained it via SCINFUL calculations [49]. Due to direct determination of ε, the PFNS, χ_s, is reported explicitly in the case of shape measurements. It is derived by an analysis,

$$\chi_s(E_{\rm inc}, E_{\rm out}) = \frac{c_s(E_{\rm inc}, E_{\rm out}) - b_s(E_{\rm inc}, E_{\rm out})}{\varepsilon_s(E_{\rm out})\tau_s(E_{\rm out})} \times m_s(E_{\rm inc}, E_{\rm out}) a_s(E_{\rm inc}, E_{\rm out}), \quad (1)$$

where a background, b_s, is subtracted from the measured counts, c_s, corrected for ε_s, multiple scattering and attenuation, m_s, angular distribution of the outgoing neutrons, a_s, and deadtime, τ_s. The subscript s indicates the sample of interest. To be exact, the measured counts, $c_s - b_s$, in Eq. (1) are given by:

$$c_s(E_{\rm inc}, \hat{E}_{\rm out}) - b_s(E_{\rm inc}, E_{\rm out}) = \sum_{i=1}^{M} R(E_{\rm inc}, \hat{E}_{\rm out}, E_{\rm out}) \times \chi_s(E_{\rm inc}, E_{\rm out})\hat{u}, \quad (2)$$

following Refs. [9, 41, 50]. The key difference here is that the multiple-scattering and attenuation correction merge with the neutron-detection efficiency to an environmental detector-response matrix, R, of the TOF measurement, while the variable $\hat{u}$ encompasses all other corrections mentioned above and not written out explicitly. It is important to stress that while one believes that the counts are measured with an energy $E_{\rm out}$, the response matrix actually distorts the true PFNS, χ, and one measures counts at $\hat{E}_{\rm out}$ due to down-scattering of outgoing neutrons. The symbol " ˆ " signifies that the outgoing-neutron energy changed due to scattering. The same is true for all other types of measurements mentioned in this section, but we follow the simplified notation in Eq. (1) as this is the way the analyses were usually undertaken in the past. This leads to a bias in the reported χ_s which will be described in the template section on ε.

2.2 PFNS Clean-ratio Shape Measurements

In a clean-ratio shape measurement, the PFNS of the investigated isotope, χ_s, is measured as ratio to a monitor spectrum, χ_m, in exactly the same set-up and environment as χ_s [18, 24, 46]. Hence, two measurements are carried out, one of χ_s and one of χ_m, as is exemplified in the middle panel of Fig. 2. Due to that, ε is expected to cancel. However, Ref. [41] shows that differing χ_s and χ_m create a difference in the total distortion (from downscattering mainly) observed for each $E_{\rm out}$. As the response contains ε and m, this difference is accounted for here in m in order to remain with the simplified notation. In addition to m, some other correction factors—background among them—reduce to the residual difference of that correction between isotope s and m. For instance, many neutron-induced experiments are measured relative to the ^{252}Cf(sf) PFNS, *e.g.*, [18,24]. While some background contributions might be similar for the measurement of the isotope of interest and the monitor one, some part of it (*e.g.*, neutron-beam-related background contributions) applies to only the neutron-induced measurement. Hence, b_s and b_m do not fully cancel but the ratio of them, b_s/b_m, is usually reduced compared to b_s. However, it is important to note that some backgrounds are subtracted before the

[1]PFNS experimental data are recommended in Ref. [1] to be treated as shapes for evaluation purposes, as their normalization (the average prompt-fission neutron multiplicity) can be often determined more precisely in dedicated measurements [48].

ratio of measurement s to m is taken, minimizing the residual effects. For instance, the neutron-beam-related background contribution can be measured with a fake fission trigger and can then be subtracted from c_s [46]. If the statistics is sufficient in the beam-background measurement, its uncertainty can be reduced to be small compared to the statistical uncertainty of the background measurement; then, the differences in the background are small from the main to the monitor spectrum. Clean-ratio shape measurements provide PFNS ratios χ_s/χ_m that then need to be converted to χ_s by using nuclear data representing χ_m. This ratio χ_s/χ_m is usually obtained by

$$\frac{\chi_s(E_{\rm inc},E_{\rm out})}{\chi_m(E_{\rm inc},E_{\rm out})} = \frac{c_s(E_{\rm inc},E_{\rm out}) - b_s(E_{\rm inc},E_{\rm out})}{c_m(E_{\rm inc},E_{\rm out}) - b_m(E_{\rm inc},E_{\rm out})} \times m_{s/m}(E_{\rm inc},E_{\rm out}) a_{s/m}(E_{\rm inc},E_{\rm out}) \tau_{s/m}(E_{\rm out}), \quad (3)$$

where the sub-script s/m reminds the reader that this factor is a residual correction effect.

2.3 PFNS Ratio-calibration Shape Measurements

The neutron-detector efficiency is derived in a PFNS ratio-calibration shape experiment from measuring χ_m in another environment and set-up than χ_s, namely:

$$\varepsilon_m(E_{\rm out}) = \frac{c_m(E_{\rm inc},E_{\rm out}) - b_m(E_{\rm inc},E_{\rm out})}{\chi_m^{ND}(E_{\rm inc},E_{\rm out})\tau_m(E)} \times m_m(E_{\rm inc},E_{\rm out}) a_m(E_{\rm inc},E_{\rm out}), \quad (4)$$

making use of nuclear data values, χ_m^{ND}, to represent χ_m. Again, two measurements are undertaken; the distinguishing factor from PFNS clean-ratio shape measurements is the different environment. Possible differences are highlighted in the lower panel of Fig. 2: The measurement might be undertaken in a different room (highlighted by red, differently sized boundaries instead of black ones) or with a different fission detector. Due to that, some correction factors do not reduce as systematically as for clean-ratio shape measurements. For instance, the room-return background depends strongly on the room and the material surrounding the sample (including potentially dissimilar fission detectors). Hence, this part of the background will not cancel for χ_s versus χ_m but needs to be determined separately as was for instance done in Ref. [19].

In some cases, ratio data χ_s/χ_m are reported for PFNS ratio-calibration shape measurements. But, sometimes χ_s is also listed in cases where the nuclear data χ_m^{ND} is accounted for in ε.

3 Information Needed for Evaluations

Sufficient experimental data are available for only a few isotopes and selected incident-neutron energies that allow to evaluate the PFNS mostly based on experimental information. The ^{252}Cf(sf) and ^{235}U(n_{th},f) PFNS [2, 3, 51] are examples of such evaluations. Even in these cases, functional forms approximating the PFNS are needed to extrapolate the evaluation based on experimental data over the whole $E_{\rm out}$ range. As mentioned in the introduction, Section 1, it is difficult to measure the PFNS below 10 keV and above 10 MeV (see also right-hand side of Fig. 1). Existing experimental data often have such high uncertainties that they are not informative for the evaluation or are not available at all. However, the PFNS needs to be given over a sufficient $E_{\rm out}$ range (usually 1.0e-5 eV to 20 or 30 MeV) to satisfy the normalization constraint and nuclear-data-format requirements [5]. Hence, functional forms approximating the PFNS—usually a Maxwellian or Watt spectrum—extending the PFNS evaluations in the tails of the spectrum are needed.

Usually, PFNS evaluations are undertaken by statistically combining model values and experimental data using associated covariances [1,8] or fitting model parameters [52–54] as was, for instance, done in ^{239}Pu(n,f) PFNS evaluations of JENDL-4.0 and JEFF-3.2 [55,56]. Many of these evaluations rely on the

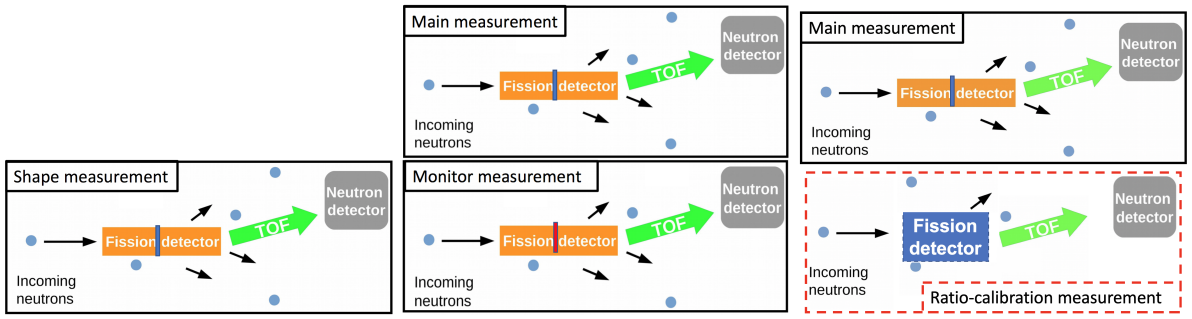

(a) Shape (b) Clean-ratio shape (c) Ratio-calibration shape

Figure 2: Schematic drawing of PFNS-measurement types. The blue rectangle in the orange fission chamber is the isotope investigated; the blue circles indicate neutrons, including the incident neutron, and scattered or background neutrons; the green arrow denotes fission neutrons headed to the neutron detector; other fission neutrons are given by the black arrows. Figure (a) is for shape measurements. Figures (b) show the main measurement (top) and the monitor measurement (bottom) for a clean-ratio shape measurements. Figures (c) show the main measurement (top) and an associated ratio-calibration measurement (bottom) made in a different experimental environment to quantify the neutron detector efficiency. Figure 3 (c-bottom) can also illustrate calibration with a spontaneous fission source such as ^{252}Cf.

original or extensions of the Los Alamos model by Madland and Nix [57], for instance, all ^{239}Pu(n,f) PFNS evaluations in ENDF/B-VII.0 to ENDF/B-VIII.0, JENDL-4.0 and JEFF-3.2 [55, 56, 58–60]. More modern models are currently under development, *e.g.*, [1, 61–63]. Models are needed for the evaluation as the experimental data of many isotopes do not cover the incident- and outgoing-neutron energy range needed for application calculations.

For an evaluation, χ_s or χ_s/χ_m is needed for the full range of incident- and outgoing-neutron energies measured. In addition to that, the temperature of a Maxwellian fitted to each χ_s (and χ_m if applicable) at a specific $E_{\rm inc}$ is needed to convert time resolution and TOF-length uncertainties given in time and length units into covariances relative to the PFNS. A fine binning of $E_{\rm inc}$ would be preferable (of 1 MeV or less), especially around second or third-chance fission thresholds to clearly resolve structures expected at these incident-neutron energies in the PFNS that are illustrated in Fig. 3. The bin size of $E_{\rm inc}$ should be quantified such that one can assign a weight to how much the measured PFNS contributes to an evaluation of a PFNS at a specific $E_{\rm inc}$. Partial uncertainties relative to the PFNS should be provided for counting statistics, δc, background corrections, δb, multiple scattering and attenuation corrections, δm, detector-response determination, $\delta\varepsilon$, nuclear data used in the analysis process, $\delta\chi_m^{ND}$, neutron-angular-distribution corrections, δa, and deadtime, $\delta\tau$. The time resolution, Δt, and TOF-length uncertainties, ΔL, are often provided either relative to energy, *e.g.*, [17, 45], or in time and length units, *e.g.*, [18, 24]. In order to convert Δt and ΔL to uncertainties relative to the PFNS, the TOF length, L, is also needed. It would be very helpful if information on the correlation coefficients of each of these partial uncertainties could be provided. However, this is rarely done, with the notable exceptions of [13, 21, 38, 39].

It is also very important to mention whether the measurement is a PFNS shape, clean-ratio or ratio-calibration shape measurement. While it is usually evident that a measurement is of the type "shape", it is not as clear to differentiate between the two ratio cases. Time resolution uncertainties in PFNS space can differ substantially at high $E_{\rm out}$ depending on whether a data set is interpreted as clean-ratio or ratio-calibration shape measurement [47]. Hence, it is very important to clearly point out in a journal article whether the ratio measurement was undertaken in the same or a very different surrounding. Related to that, if a specific nuclear-data set, *e.g.*, the ^{252}Cf(sf) PFNS by [2, 3], was used

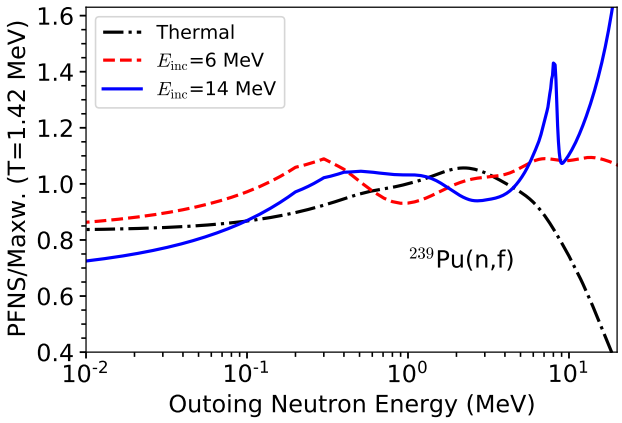

Figure 3: ENDF/B-VIII.0 ^{239}Pu PFNS [8, 58] are used as examples to illustrate structures commonly observed around second- and third-chance fission thresholds: From thermal E_{inc} to the on-set of second chance fission, curves similar in shape to the thermal PFNS are expected. In a window of E_{inc}=1–2 MeV around second-chance fission (red dashed line), one sees a characteristic structure of the PFNS appear in the 100s of keV stemming from a second-chance fission contribution to the PFNS that is only non-zero up to these energies due to energy conservation. Around the third-chance fission threshold (blue solid line), this structure is like a broader shoulder in E_{out} above 100 keV. One also sees a sharp structure at high E_{out} (several MeV) coming from the pre-equilibrium neutron emission from the compound nucleus before fission happens.

to convert ratio to shape data, this data set should be clearly cited. If not readily available nuclear data but rather a custom-reference data set was used for the conversion, this should be provided explicitly in the journal publication, as was done in Ref. [24], in order to be able to convert to shape data with the newest available reference data.

Auxiliary information on the experiment (such as set-up information, isotopic content of sample, *etc.*) is rarely used explicitly in the evaluation process. However, its importance should not be underestimated. If auxiliary information describing the experiment in detail is provided, the data can be simulated and re-analyzed at a later time, often providing key input to understand discrepancies between existing data sets [9] that can have significant impact on application calculations [7]. This kind of information comprises all details that describe the experiment and allows one to simulate it: For instance, MCNP input decks, tabulated values of all pertinent correction factors, raw data, schematic drawings, sample thickness, isotopic composition, and dimension of all materials in the beam that could potentially produce neutrons.

4 Template

A listing of all uncertainty sources relevant for PFNS TOF measurements is provided below, along with the template values in Tables I and II. All uncertainties are given relative to the PFNS in % unless otherwise noted.

Counting-statistics Uncertainties No counting-statistic uncertainties, δc, are provided in the template. These values depend strongly on the measurement time, neutron flux, detector response and set-up. Hence, δc is hard to estimate. In addition to that, we take the approach of recommending to reject a data set if this very basic uncertainty information cannot be obtained for it. The correlation matrix associated with δc is usually diagonal for PFNS data measured within the same experiment (independent of incident- and outgoing-neutron energy) and not correlated to other measurements.

Table I: Typical uncertainty sources encountered in PFNS measurements are listed dependent on their specific measurement type. Also, estimates of typical uncertainty ranges are provided in case this information cannot be derived otherwise for uncertainty-quantification purposes. "ND" was used as abbreviation for nuclear data.

Unc.	Shape (%)	Clean-ratio shape (%)	Ratio-calibration shape (%)
δc	Must be provided	Must be provided (δc_s & δc_m)	Must be provided (δc_s & δc_m)
δb	0.2–3	0.2–2	0.2-3 for both
δm	1–20 (not corrected)	0.1–5 (not corrected)	1–20 (not corrected, both)
	0.1–3 (corrected)	0–0.8 (corrected)	1–3 (corrected, both)
$\delta\varepsilon$	2–7 (efficiency)	Cancels	Unc. in determining χ_m
	0–10 (response not folded)	-	0-10 both (response not folded)
δa	0.1	0.1	0.1
$\delta\tau$	0.1	0.1	0.1 for both
ND	0.1–5 (simulations)	0–0.5 (simulations)	0.1–5 both (simulations)
	-	From libraries (reference)	From libraries (reference)
δt	2.5 ns	2.5 ns both	2.5 ns both
ΔL	2 mm	2 mm both	2 mm both
$\delta\omega$	Impurity-level dependent	Both samples	Both samples

Background Uncertainties Careful background corrections are an essential part of a PFNS measurements. The background, b, can assume values at some E_{out} that are even larger than the signal one wants to measure [9]. This is especially true at $E_{\text{out}} < 100$ keV [13,36,40,50,64]. Background can arise from γs in γ-sensitive neutron detectors, beam contaminations (*e.g.*, secondary-neutron group, protons or charged particles in the beam), wrap-around neutrons (dependent on spacing between source-neutron pulses), from pile-up of incident neutrons, room-return, random coincidences, α-particles from the sample, *etc.* Adequate shielding and background analysis can effectively reduce b and δb. Also, coincidence backgrounds can be measured directly with the insertion of a trigger or signal that is random in time (*i.e.*, random when comparing the time difference between the trigger and real fission events) [46,65]. Typical background uncertainties are in the range of 0.2–3% from 0.1–10 MeV and can rise up to $\delta b \sim$ 50% at 10 keV in shape measurements [14,15,18,25]. These values are recommended to be used in the template along with a Gaussian correlation shape to account for correlations between δb. A Gaussian shape across outgoing- and incident-neutron energies was chosen because sometimes nuclear data are used in the background-correction process or separate measurements were performed that brings a combination of statistical and systematic effects [13,19]. This approximate functional form is chosen in lieu of knowing the more complicated correlation matrices that can be obtained by experimentalists for their own measurement. It should be highlighted that background uncertainties can change with E_{out} and E_{inc} given that incident-neutron background can also contribute. Correlations between δb of different experiments can be non-zero if the same methods were used to correct for b or both measurements were undertaken at the same facility.

In clean-ratio shape measurements, the correction of b is partially reduced as some background constituents (*e.g.*, room return) are the same for both measurements for each individual outgoing-neutron energy, though the collection of counts at each TOF may be differently impacted by room return based on differences in the outgoing neutron spectrum. However, if one of the measurements was undertaken with the neutron beam on and the other off, the beam-related contributions to b will not reduce, unless corrected separately as mentioned above. This case is often applicable to ratio measurements as many neutron-induced PFNS are measured relative to the spontaneously fissioning ^{252}Cf spectrum. Hence, a smaller δb of 0.2–2% is recommended for clean-ratio shape measurements. The uncertainty for δb of shape measurements applies twice to δb of ratio-calibration shape measurements, due to the different

Table II: Typical uncertainty sources encountered in PFNS measurements are tabulated with special emphasis on shapes of correlations. "ND" was used as abbreviation for nuclear data.

Unc.	Cor(Exp_i,Exp_i)	Cor(Exp_i, Exp_j) $i \neq j$
δc	Diagonal	None
δb	Gaussian	Facility and method dependent
δm	Gaussian anti-correlated around 2T	Facility and method dependent
$\delta\varepsilon$	Gaussian	Depends on ε determination
δa	Gaussian	Gaussian
$\delta\tau$	Full	0
ND	From libraries	From libraries
δt	From TOF $\rightarrow E_{\text{out}}$ transformation	0
ΔL	From TOF $\rightarrow E_{\text{out}}$ transformation	0
$\Delta\omega$	Dependent on shape difference between main and impurity PFNS	Sample/ method dependent

environmental conditions of the two experiments.

Multiple-scattering and Attenuation Uncertainties Corrections for multiple scattering and attenuation are two key factors that must be diligently addressed in each PFNS measurement. The reason is that one measures outgoing neutrons, which commonly down-scatter in surrounding material, leading to a sizable correction. The correction itself depends on the geometry and isotopic composition of the target and of the experimental environment. If samples are thick, as for instance in [17, 45], the multiple-scattering correction can amount to 10–20% [9]. Also, scattering in surrounding material can be significant [7, 9], leading to combined corrections in the maximum range of 20%. The absolute size depends on the geometry of and isotopes in the surrounding material. The larger the amount of material present, the larger m is expected to be. However, some isotopes have larger neutron-scattering and neutron-capture cross sections than others leading possibly to larger corrections than are necessary for isotopes that are more abundant but have small neutron-scattering or capture cross sections. If this scattering effect is corrected by using neutron-transport simulations, *e.g.*, as done in [13, 18], the uncertainties of underlying nuclear data dependent on E_{out} and E_{inc} of neutrons will contribute to δm. The multiple-scattering correction shows a clear E_{out} dependence: It is usually largest at low E_{out} where the PFNS is small to begin with and many neutrons down-scatter over time, while it becomes negligibly small around the peak region, and above, of the PFNS [7, 9]. To be clear, neutrons down-scatter from higher outgoing-neutron energies, but their percentage is small compared to the non-scattered neutrons making the correction small around the peak. The PFNS at low outgoing-neutron energies is small, leading to a larger relative percentage of down-scattered neutrons, and therefore a larger uncertainty, δm, in the correction factor. Hence, we recommend for the template 20% for shape measurements at 10 keV linearly decreasing to 1% at the peak region of the PFNS, if this correction has not been applied. However, at the same time, we caution to critically assess whether this missing correction factor might not adversely bias the evaluated results. If that is the case, it might be better to attempt a correction for m based on detailed simulations or reject the data altogether before assigning such a large missing uncertainty. If m was corrected but δm is missing, δm could be estimated to be 10–20% of the correction factor which is given here with 0.1–3% for shape data. As the shapes change with E_{inc}, so does m. However, these differences are secondary effects leading to no incident-neutron-dependent template values.

In clean-ratio shape measurements, m reduces to the different response of χ_s compared to χ_m to this effect. If χ_s and χ_m are very similar, m and, hence, δm can become small [23, 24, 41]. If χ_s and

χ_m differ significantly, a systematic bias can amount to a value of a few per-cent across the majority of the PFNS range, with corrections on the order of 10% or more possible near pre-equilibrium neutron emission regions [41]. If an $m \neq 1$ due to systematic differences of χ_s and χ_m is not corrected for, δm would assume this value. This is, for instance, the case for a PFNS measured with incident neutrons of an energy right at the second-chance-fission threshold as a ratio to the ^{252}Cf(sf) spectrum. The ^{252}Cf spectrum is smooth in Fig. 1, while clear structures in PFN spectra at the second-chance fission thresholds have been observed [1, 13, 46] which are illustrated in Fig. 3. Marini *et al.* estimated the maximum of this effect to be 2% in an analysis of their measurement [46], while Kelly *et al.* showed this effect to be up to 5% for distinctly different χ_s and χ_m at the second-chance fission threshold using a different fission detector [38, 41]. The latter publication also showed that this effect is isotope dependent and does not vanish at any studied $E_{\rm inc}$ if χ_s and χ_m differ. Marini *et al.* measured a ^{239}Pu PFNS in ratio to ^{252}Cf(sf), which are closer in mean energy than ^{235}U PFNS for many $E_{\rm inc}$, hence, the effect observed was smaller than the maximum of 5% observed in Ref. [41]. We take the latter value, 5%, as the upper template value for clean-ratio shape measurements for PFNS not corrected by m. The discussion above also illustrates that m depends on the outgoing-neutron energy along with the incident-neutron energy as structures in the PFNS, and, therefore, differences to the ^{252}Cf(sf) spectrum, arise contingent upon the incident-neutron energy. Again, 15% of that effect is assumed as uncertainty value if the effect was corrected but no other information was supplied to estimate the uncertainties.

In ratio-calibration shape measurements, m needs to be determined for both measurements, because χ_m and χ_s were determined in dissimilar surroundings, and, hence, the correction is different. A dissimilar surrounding could be, for instance, significantly different sample sizes, different fission-detector dimensions and materials, different room and shielding configurations. Of course, using a ^{252}Cf sample instead of ^{235}U is in itself dissimilar as both have a different PFNS, but this case falls under the clean-ratio shape category if all other measurement components are the same. For the ratio-calibration shape technique, δm in the template is estimated by using the respective value for shape measurements and apply it to provide an uncertainty for both, δm_s and δm_m, leading to an overall larger uncertainty contribution. Of course, this is a strong approximation taken because of missing information.

Usually, these multiple-scattering effects are simulated or calculated with neutron-transport codes of varying sophistication [12, 13, 66]. Attempts were undertaken in only a few rare cases to measure this effect [24]. The accuracy of m depends on uncertainties of nuclear data used in the codes, the accuracy of the set-up description used in the simulation, the accuracy of the physics model used for the simulation and finally Monte Carlo counting statistics. The latter uncertainties are expected to be small compared to the other components which would lead to strong correlations. Therefore, a Gaussian shape is assumed across outgoing-neutron energies that is strongly correlated between incident-neutron energies. An anti-correlated shape around the turning point of the PFNS (around the maximum of χ_s) is assumed given the fact that neutrons down-scatter (*i.e.*, are lost) in the higher energy range and are added to a lower one. The Chi-Nu team investigated the location of this turning point for the scattering-correction factors in their measurement and showed that it appears between 3–4 MeV for ^{239}Pu PFNS dependening on the exact detector array used [13, 50], supporting a value of about two times the Maxwellian. Their multiple-scattering correction is a convoluted correction containing also detector efficiency, yielding a response function R as given in Eq. (2).

Correlations between δm of different experiments can arise if the same codes/ methods, nuclear data and similar materials have been used for correcting m. Then this correlation matrix can be assumed to be Gaussian with an overall smaller correlation factor compared to correlations for δm between the same experiment.

Detector-response Uncertainties The detector-response uncertainties, ε, should be explicitly given for shape measurements. It is often termed "detector-efficiency" uncertainty [14–17, 45]. Here,

the term "response" is used to highlight that, indeed, there is no one-to-one correspondence of TOF to $E_{\rm out}$ as also shown in Eq. (2) with the response function R. To be more specific, multiple-scattering effects lead to a response function that couples one specific TOF with several ("true" initial) $E_{\rm out}$-bins [9, 41]. Taddeucci *et al.* showed in Figs. 4 and 5 of Ref. [9] that multiple scattering distorts a simulated PFNS at at low and high $E_{\rm out}$; the large distortion at low $E_{\rm out}$ is driven by down-scattering from a much larger peak. At higher $E_{\rm out}$, neutrons scatter down and the response gets increasingly more uncertain as the finite time resolution plays an increasing effect. This increase above the peak seen in Figs. 4 and 5 of Ref. [9] is used to estimate a detector-response uncertainty to be 0% below $E_{\rm out}$ = 2 MeV, linearly rising to 10% at 10 MeV [7,8]. This uncertainty applies to shape measurements, which did not take this effect into account. It can be corrected for by neutron-transport simulations along with scattering corrections. This detector-response uncertainty is in addition to those uncertainties usually reported as related to detector "efficiency". The latter uncertainties are often in the range of 2–7% [14–17,45] across relevant measurements. These values are used here as a range for the template. This uncertainty stems from reference nuclear data used to measure or simulate ε. The uncertainties in ε become large where either these nuclear data are not well-known or at the threshold of the respective detector. As $\delta\varepsilon$ is related to transformed nuclear-data uncertainties, a Gaussian shape is used for correlations between $\delta\varepsilon$ of the same experiment. If the same detector-response function is assumed for different $E_{\rm inc}$ [45], $\delta\varepsilon$ is fully correlated for PFNS at different $E_{\rm inc}$ but the same $E_{\rm out}$ values. Non-zero correlations between $\delta\varepsilon$ of different experiments arise from common usage of the same nuclear data. If the same nuclear data were likely used, a Gaussian shape can be used. If ε determinations of two experiments are related to obviously different and uncorrelated nuclear data, the correlations between $\delta\varepsilon$ are zero.

One would expect ε to drop out in clean-ratio shape measurements. The ratio procedure—dividing measured main isotope through ^{252}Cf outgoing-neutron counts and then multiplying by PFNS nuclear data for the latter isotope—applies scattering and efficiency (intrinsic detector response) at the same time. ε cancels only then if both χ_m and χ_s are measured in exactly the same environment *and* the two PFNS (and thus m_s and m_m) are identical. If χ_m and χ_s are substantially different, a sizable difference can be observed [41] in the detector responses to both PFNS. The uncertainty related to this effect is accounted for in the template in δm for clean-ratio shape measurements.

Ratio-calibration measurements aim at determining ε via measuring χ_m. Hence, the uncertainties of ε for this measurement type are made up of all uncertainties determining χ_m, including the related nuclear-data uncertainties. It is preferable that all uncertainties related to measuring χ_m are provided instead of $\delta\varepsilon$. Hence, no separate template value is given for that. However, it should be mentioned that the detector response measured via χ_m might actually not be the same as for the χ_s measurement. A difference can arise due to the different surrounding, fission detector and sample size (^{252}Cf samples are often point-source). This difference should be quantified.

Angular-distribution Uncertainties The uncertainties related to correcting for the angular distribution of neutrons, δa, are expected to be small in many measurements. An angular bias can be introduced in measurements if the fission-fragment detector has a restricted angular coverage (*e.g.*, in the case of a parallel-plate avalanche counter) and is coupled with neutron detectors that cover only part of the angular range. Fission fragments were shown to have a non-isotropic angular distribution even below 1 MeV for many actinides [67–69]. However, the resulting neutrons in the lab frame are less strongly-forward peaked until the on-set of the pre-equilibrium neutron-emission contribution to the PFNS [37]. This pre-equilibrium neutron-emission forward peak (at a few MeV in the blue solid line of Fig. 3) starts to emerge around $E_{\rm inc}$ = 10 MeV for most actinides. If the neutron detectors do not cover 2π, a substantial bias in χ_s might be introduced in this $E_{\rm inc}$ range due to the restricted angular coverage. This bias has the potential to render data unusable for evaluations [8] as was the case for [10,12]. However, one can expect the bias introduced and δa to be small for lower $E_{\rm inc}$ [37,46] unless an unfavorable set-up leads to angular bias (see Ref. [1, 25] for examples of those). One possibility to

minimize a potential angular bias is to measure neutrons across a large angular coverage.

It is expected that ^{252}Cf(sf) prompt-fission neutrons are isotropically distributed. Hence, even if one measures as a ratio to the ^{252}Cf(sf) spectrum, a potential bias will not drop out. The only issue that could lead to an-isotropic prompt-fission neutrons from ^{252}Cf(sf) is that fission fragments emitted at shallow angles in the sample might remain in the sample, which could distort the start signal of the PFNS. This effect could cancel out if the ^{252}Cf and main measurements are undertaken in the same experimental set-up (*i.e.*, same design of fission chamber and dimensions of targets).

A small uncertainty value of 0.1% is recommended for δa in Table I. This should serve as a reminder to question whether an unfavorable set-up could potentially bias a PFNS measurements. It should be understood that this effect can be very different at thermal energies compared to, *e.g.*, 20 MeV incident-neutron energies. This effect would be usually corrected by simulating it via neutron-transport codes, or extrapolating experimental angular distributions, if a sufficient number of angles are covered. Correlations across uncertainties at different $E_{\rm inc}$, $E_{\rm out}$ and even different experiments could result from common usage of nuclear data and physics models. Hence, similarly to δm, Gaussian correlation shapes are assumed.

Deadtime Uncertainties Dead-time effects matter for measurements with high count rates compared to the detector or data data-acquisition systems integration times. No signal is measured, *i.e.*, the detector is "dead", from the time it triggers to the end of the signal-integration window. Deadtime can be minimized in measurements by reducing the count rate per detector using appropriately small samples or detectors. Also, the choice of the detector type can help suppress deadtime effects to a negligible amount; Liquid scintillators and Li-glass scintillators should, for instance, be fast enough to control deadtime effectively. In addition, the use of waveform digitizers, now common in many laboratories, allows significant reduction in deadtime corrections. In past measurements, deadtime was also reduced by making the neutron detector the start-signal, while making the fission counter the stop signal (that fires more often) by delaying the latter [6, 42–44]. Hence, a small uncertainty, $\delta\tau$ of 0.1%, is recommended in the template for all measurement types with a full correlation between $\delta\tau$ assuming that the effect would affect all PFNS similarly. No correlation is assumed for $\delta\tau$ between experiments given that often different equipment, sample sizes, *etc.*, are used.

Nuclear-data Uncertainties There are two sources of possible nuclear-data uncertainties. The first one appears in ratio measurements. χ_m needs to be known either to determine ε (ratio-calibration shape measurements, see Eq. (4)) or to convert ratio data to χ_s (clean-ratio shape data). These uncertainties are usually straight-forward to estimate if one knows what data were used for χ_m in Eq. (4) or if ratio data are explicitly provided rather than a derived χ_s. The latter case is actually preferred as it gives evaluators the possibility to use the currently best available nuclear data for χ_m.

Once the exact data that were used to represent χ_m are known, their associated covariances can be retrieved from the relevant database and used directly in the uncertainty procedure. Hence, it is of high importance to clearly state which specific nuclear data (*e.g.*, library reference) were used for the conversion of ratio to shape data. If ratio data were converted to shape data by using a simple functional form representing the reference PFNS, such as for instance a Maxwellian, the parameters of this function need to be documented. This specific uncertainty source can lead to non-negligible correlations between PFNS covariances of different experiments and across different $E_{\rm inc}$ if they were all measured relative to the same observable. However, these are again straight-forward to estimate.

The second source of nuclear-data uncertainties relates to the fact that nuclear data are frequently used for many corrections to χ_s. One example is that nuclear data are used in neutron-transport codes to calculate m. This nuclear-data related uncertainty source was estimated in only rare cases [38,39,70]. This uncertainty amounted to values of 0.1–5% for Chi-Nu data. These values were calculated by forward-propagating the ^{6}Li(n,t) cross-section covariances used in the MCNP simulations of the Chi-Nu assembly to PFNS uncertainties by using the implicit-capture capability of MCNP-6.2 [70, 71].

These uncertainties are listed in the template, but are only applicable to measurements using Li-glass scintillators. These values serve as a reminder for the reader that additional nuclear-data uncertainties should apply if neutron-transport simulations based on nuclear data are used in the measurement analysis. However, more detailed studies are needed across many measurements and nuclear-data observables. It is expected that these uncertainties reduce in clean-ratio shape measurements as the same materials are used in both experiments. The only difference is related to the response of χ_m compared to χ_s to the surrounding material. One could assume that this residual effect is a tenth of the original effect. In ratio-calibration shape measurements, this effect and related uncertainty would need to be estimated twice because of the dissimilar materials.

Time-resolution Uncertainties Time-resolution values, Δt, from 0.5 to 5 ns can be found across many TOF measurements, *e.g.*, [10,12,13,18,19,24,25], with many experiments reporting 1–2 ns. If no value is provided, a value of 2.5 ns is recommended. If the detector type is known, one can compare to typical time resolutions of the specific detector type. It is chosen slightly more conservative then the mean of these bounding values. This value applies to shape measurements and can be used for both, χ_s and χ_m, for the two ratio types.

The correlation matrix shape for this uncertainty for the same measurement arises from the conversion of TOF to E_{out} and then to an uncertainty relative to the PFNS as is described in [47]. This correlation factors can be derived across incident- and outgoing-neutron energy for Δt. The absolute size of uncertainties related to Δt in PFNS space depends strongly on the measurement type used to obtain χ_s. A Maxwellian temperature T or Watt parameters fitted to χ_s (and χ_m if applicable) are needed for this conversion along with the TOF length L. The TOF length needs to be measured between the sample and the neutron detector(s). The spectrum parameters can be fitted by the evaluators themselves if need be. However, L must be provided by the experimentalists. This is especially the case for shape and ratio-calibration shape measurements, as δt can be a dominant uncertainty source at $E_{\text{out}} > 8$ MeV.

Usually, the time resolution is estimated from the width of the peak caused by prompt gamma rays created in the fission process. This triggers the start signal for the TOF measurement of the outgoing neutrons. This determination is assumed to be independent from one measurement to another. Hence, zero correlation is assumed between δt of two experiments unless they were performed by the same team in the same facility. An example of that is the measurement series encompassing [11, 22–24].

TOF-length Uncertainties The TOF-length uncertainty, ΔL, usually leads to a minor uncertainty source contributing to the total PFNS covariances. Its values range from 1–5 mm across the literature [11, 13, 18, 19, 22–25] with most values closer to 1 mm. Hence, a value of 2 mm was chosen for the template. It needs to be considered once for the shape measurement and twice, for χ_s and χ_m, in the case of ratio measurements. Again, a Maxwellian temperature or Watt parameters fitted to the measured PFNS should be and a TOF length must be provided in order to transform ΔL into an uncertainty relative to the PFNS. The correlation-matrix shape between the transformed ΔL uncertainties of the same experiment across E_{out} and E_{inc} arises again from this conversion process. Similarly to Δt, we assume that correlations are zero between uncertainties stemming from ΔL between different experiments. This assumption is made as the determination of L is usually independent between different experiments and a bias would be randomly distributed across them.

Impurity Uncertainties The impurity uncertainties depend on the actual level of impurities in the sample. If the samples are of very high purity, $> 99.9\%$ of fissionable material, the impurity uncertainty on the PFNS is negligibly small. For subthreshold measurements of PFNS (uncommon), impurities that have a lower fission threshold can be more important. Also, impurity uncertainties can become sizable if the sample contaminations are not well known. This is also true when samples are re-used.

In this case the current composition needs to be calculated starting from the date the sample was last chemically cleaned.

A correction of the sample impurity would depend on the level of the contamination as well as nuclear data of the impurity versus the main isotope. To be more precise, one needs to know how likely it is that the impurity fissions, how many neutrons are emitted and how much its PFNS differs from nuclear-data values of the main constituent of the sample. The differences in fission cross section and neutron multiplicity would be only dependent on the incident-neutron energy, while the PFNS difference would lead to a correction factor dependent also on the outgoing-neutron energy. Hence, the correlation shape across E_{out} and E_{inc} could be estimated as strongly correlated but not fully because of the dependence on the difference between the PFNS of the main and impurity isotope.

Correlations between impurity uncertainties of different measurements can arise if the same sample was used. Even if different samples with similar contaminants were used, the impurity uncertainty can be strongly correlated (correlation coefficient of 0.5–0.75) between experiments if the same nuclear data are used for the correction and the same method was used to measure the impurity level.

5 Conclusions

Templates of expected measurement uncertainties were established here for prompt fission neutron spectra (PFNS). These templates list expected uncertainty sources for each distinct PFNS measurement type (shape, clean-ratio, and indirect ratio measurements). They also give ranges of uncertainties for most sources and estimates of correlation coefficients between uncertainties of each source. The uncertainty values were estimated conservatively, unless otherwise noted, based on information found for a broad range of experiments in their literature or respective EXFOR entries as well as expert judgment from experimenters. In addition to these templates, a section is provided that lists what evaluators need to include experimental PFNS faithfully into the evaluation process.

Conflicts of Interest

The authors declare that they have no competing interests to report.

Funding

We gratefully acknowledge partial support of the Advanced Simulation and Computing program at LANL. This work was supported by the US Department of Energy through the Los Alamos National Laboratory. Los Alamos National Laboratory is operated by Triad National Security, LLC, for the National Nuclear Security Administration of the US Department of Energy under Contract No. 89233218CNA000001. This material benefited from work supported by the U.S. Department of Energy, Office of Science, Office of Nuclear Physics, under the Nuclear Data InterAgency Working Group Research Program.

Data availability statement

The data that were created associated with the manuscript are all within its main text and tables.

Author contribution statement

DN wrote the original draft, MD and PM contributed text to that. All authors reviewed and proposed edits to the manuscripts. All authors were involved in investigations and data curation associated with

the article and discussions on uncertainty quantification for PFNS.

References

[1] R. Capote, Y.-J. Chen, F.-J. Hambsch *et al.*, "Prompt Fission Neutron Spectra of Actinides," Nucl. Data Sheets **131**, 1–106 (2016).

[2] W. Mannhart, "Evaluation of the Cf-252 Fission Neutron Spectrum between 0 MeV and 20 MeV," IAEA Report IAEA-TECDOC-410, 158–171 (1987).

[3] W. Mannhart, "Status of the Cf-252 Fission Neutron Spectrum Evaluation with Regard to Recent Experiments," IAEA Report INDC(NDS)-220, 305–336 (1989).

[4] A.D. Carlson, V.G. Pronyaev, R. Capote *et al.*, "Evaluation of the Neutron Data Standards," Nucl. Data Sheets **148**, 143–188 (2018).

[5] A. Trkov, M. Herman and D.A. Brown (Eds.), "ENDF-6 Formats Manual," Brookhaven National Laboratory Report BNL-90365-2009 Rev.2 (2012).

[6] A. Chalupka, L. Malek, S. Tagesen *et al.*, "Results of a Low-background Measurement of the Fission Neutron Spectrum from ^{252}Cf in the 9- to 29-MeV Energy Range," Nucl. Sci. Eng. **106**, 367–376 (1990).

[7] D. Neudecker, T.N. Taddeucci, R.C. Haight *et al.*, "The Need for Precise and Well-documented Experimental Data on Prompt Fission Neutron Spectra from Neutron-induced Fission of ^{239}Pu," Nucl. Data Sheets **131**, 289–318 (2016).

[8] D. Neudecker, P. Talou, T. Kawano *et al.*, "Evaluations of Energy Spectra of Neutrons Emitted Promptly in Neutron-induced Fission of ^{235}U and ^{239}Pu," Nucl. Data Sheets **148**, 293-311 (2018).

[9] T.N. Taddeucci, R.C. Haight, H.Y. Lee *et al.*, "Multiple-scattering Corrections to Measurements of the Prompt Fission Neutron Spectrum," Nucl. Data Sheets **123**, 135–139 (2015).

[10] G.S. Boikov, V.D. Dmitriev, G.A. Kudyaev *et al.*, "Spectrum of Neutrons Accompanying Fission of ^{232}Th, ^{235}U, and ^{238}U by 2.9-MeV and 14.7-MeV Neutrons (Below and Above the Threshold of Emission Fission)," Sov. J. Nucl. Phys. **53**, 392–405 (1991), EXFOR-No. 41110.009.

[11] A.A. Boytsov, A.F. Semenov and B.I. Starostov, "Relative Measurements of ^{233}U+n_{th}, ^{235}U+n_{th} and ^{239}Pu+n_{th} Prompt Fission Neutron Spectra (PFNS) in the Energy Range 0.01–5 MeV," IAEA Report INDC(CCP)-0459 (2014); translation into English from: in *Proceedings of the All-Union Conf. on Neutron Physics, Kiev, USSR,* **2**, pp. 294–297 (1983), EXFOR-No. 40873.006 for ^{239}Pu and 40873.004 for ^{235}U.

[12] A. Chatillon, G. Bélier, T. Granier *et al.*, "Measurement of Prompt Neutron Spectra from the ^{239}Pu(n, f) Fission Reaction for Incident Neutron Energies from 1 to 200 MeV," Phys. Rev. C **89**, 014611 (2014), EXFOR-No. 14379.

[13] M. Devlin, J.A. Gomez, K.J. Kelly *et al.*, "The Prompt Fission Neutron Spectrum of ^{235}U(n,f) below 2.5 MeV for Incident Neutrons from 0.7 to 20 MeV," Nucl. Data Sheets **148**, 322–337 (2018).

[14] M.M. Islam and H.-H. Knitter, "The Energy Spectrum of Prompt Neutrons from the Fission of Uranium-235 by 0.40-MeV Neutrons," Nucl. Sci. Eng. **50**, 108–114 (1973), EXFOR-No. 20385.003.

[15] P.I. Johansson and B. Holmqvist, "An Experimental Study of the Prompt Fission Neutron Spectrum Induced by 0.5-MeV Neutrons Incident on Uranium-235," Nucl. Sci. Eng. **62**, 695–708 (1977), EXFOR-No. 20175.003.

[16] H.-H. Knitter, M.M. Islam and M. Coppola, "Investigation of Fast Neutron Interaction with ^{235}U," Z. Phy. **257**, 108–123 (1972), EXFOR-No. 20394.008.

[17] H.-H. Knitter, "Measurement of the Energy Spectrum of Prompt Neutrons from the Fission of Pu239 by 0.215 MeV Neutrons," Atomkernenerg. **26**, 76–79 (1975), EXFOR-No. 20576.003.

[18] N. Kornilov, F.-J. Hambsch, I. Fabry *et al.*, "The ^{235}U(n,f) Prompt Fission Neutron Spectrum at 100K Input Neutron Energy," Nucl. Sci. Eng. **165**, 117–127 (2010), EXFOR-No. 31692.006.

[19] A. Lajtai, J. Kecskeméti, J. Sáfár *et al.*, "Energy Spectrum Measurements of Neutrons for Energies 30 keV–4 MeV from Thermal Fission of Main Fuel Elements," Proceedings of the Conf. on Nuclear Data for Basic and Applied Sciences, Santa Fe, USA, 1985, **Vol. 1**, 613–616 (1985), EXFOR-No. 30704.004.

[20] J.P. Lestone and E.F. Shores, "Uranium and Plutonium Average Prompt-fission Neutron Energy Spectra (PFNS) from the Analysis of NTS NUEX Data," Nucl. Data Sheets **119**, 213–216 (2014).

[21] J.P. Lestone and E.F. Shores, "Uranium and Plutonium Prompt-fission-neutron Spectra (PFNS) of NTS NUEX Data and the Corresponding Uncertainty Budget," Los Alamos National Laboratory Report LA-UR-14-24087 (2014).

[22] V.N. Nefedov, B.I. Starostov and A.A. Boytsov, "Precision Measurements of ^{252}Cf, ^{233}U, ^{235}U and ^{239}Pu Prompt Fission Neutron Spectra (PFNS) in the Energy Range 0.04–5 MeV," IAEA Report INDC(CCP)-0457 (2014); translation into English from: in *Proc. of the All-Union Conf. on Neutron Physics, Kiev, USSR*, **2**, 285–289 (1983), EXFOR-No. 40871.009 for ^{239}Pu and 40871.007 for ^{235}U.

[23] B.I. Starostov, V.N. Nefedov and A.A. Boytsov, "Precision Measurements of ^{252}Cf, ^{233}U+n_{th}, ^{235}U+n_{th} and ^{239}Pu+n_{th} Prompt Fission Neutron Spectra (PFNS) in the Energy Range 2–11 MeV," IAEA Report INDC(CCP)-0458 (2014); translation into English from: in *Proc. of the All-Union Conf. on Neutron Physics, Kiev, USSR*, **2**, 290–293 (1983), EXFOR-No. 40872.003 for ^{239}Pu and 40872.007 for ^{235}U.

[24] B.I. Starostov, V.N. Nefedov and A.A. Boytsov, "Prompt Neutrons Spectra from the Thermal Neutron Fission of ^{233}U, ^{235}U, ^{239}Pu and Spontaneous Fission of ^{252}Cf in the Secondary Neutron Energy Range 0.01–12 MeV," IAEA Report INDC(CCP)-293/L, 19–32 (1989), translation into English from: Nucl. Constants, **3**, 16 (1985), EXFOR-No. 40930.008.

[25] A.S. Vorobyev and O.A. Shcherbakov, "Integral Prompt Neutron Spectrum for Fission of ^{235}U by Thermal Neutrons," IAEA Report INDC(CCP)-0455, 21–41 (2014), EXFOR-No. 41597.002.

[26] V.Ya. Baryba, N.V. Kornilov and O.A. Sal'nikov, IPPE Report 947 (1979) (in Russian), available in INIS, EXFOR 40740.

[27] B.V. Zhuravlev, L.E. Kazakov, V.J. Kononov *et al.*, "Investigations of the Interactions of Neutrons with ^{238}U Nuclei,"IAEA Report INDC(CCP)-154/L (1980).

[28] M. Baba, H. Wakabayashi, M. Ishikawa *et al.*, "Fission Spectrum Measurement of ^{232}Th and ^{238}U for 2 MeV Neutrons,"in *IAEA Consult. Meet. on Physics of Neutron Emission in Fission, Mito, Japan*, IAEA Report INDC(NDS)-220, pp.149–159 (1989), EXFOR 22112.

[29] G.S. Boykov, V.D. Dmitriev, G.A. Kudyaev *et al.*, "Spectrum of Neutrons Accompanying Fission of ^{232}Th, ^{235}U, and ^{238}U by 2.9-MeV and 14.7-MeV Neutrons (Below and Above the Threshold of Emission Fission)," YAD. FIZ. **53**, 628–648 (1991); original: SOV. J. NUCL. PHYS. **53**, 392–406 (1991), EXFOR 41110.

[30] G.S. Boykov, V.D. Dmitriev, G.A. Kudyaev *et al.*, "New Data on Prefission Neutrons", Z. PHYS. **A340**, 79–84 (1991).

[31] G.S. Boykov, V.D. Dmitriev, G.A. Kudyaev *et al.*, "Neutron spectrum in the fission of Th-232, U-235, and U-238 by neutrons with energies 2.9 and 14.7 MeV," PHYS. ATOMIC NUCL. **57**, 572 (1994).

[32] G.N. Smirenkin, G.N. Lovchikova, A.M. Trufanov *et al.*, "Measurement of Energy Spectrum of Neutrons Accompanying Emission Fission of U-238 nuclei," YAD. FIZ. **59**, 1934–1939 (1996); original: PHYS. AT. NUCLEI **59**, 1865–1870 (1996), EXFOR 41461.

[33] A.M. Trufanov, G.N. Lovchikova, M.I. Svirin *et al.* "Investigation of the Spectra of Neutrons Originating from ^{238}U Fission Induced by 5.0- and 13.2-MeV Neutrons," YAD. FIZ. **64**, 3–10 (2001); original: PHYS. AT. NUCLEI **64**, 1–8 (2001), EXFOR 41450.

[34] G.N. Lovchikova, A.M. Trufanov, M.I. Svirin *et al.*, "Spectra and Mean Energies of Prompt Neutrons from ^{238}U Fission Induced by Primary Neutrons of Energy in the Region $E_n < 20$ MeV," YAD. FIZ. **67**, 1270–1287 (2004); original: PHYS. AT. NUCLEI **67**, 1246–1263 (2004), EXFOR 41447.

[35] Experimental Nuclear Reaction Data Library (EXFOR), IAEA Nuclear Data Section. See https://www-nds.iaea.org/exfor (accessed on 8/11/2016), or for the NNDC at Brookhaven National Laboratory, the mirror site is http://www.nndc.bnl.gov/exfor (accessed on 8/11/2016); N. Otuka, E. Dupont, V. Semkova *et al.*, "Towards a More Complete and Accurate Experimental Nuclear Reaction Data Library (EXFOR): International Collaboration Between Nuclear Reaction Data Centres (NRDC)," NUCL. DATA SHEETS **120**, 272–276 (2014); V.V. Zerkin and B. Pritychenko, "The Experimental Nuclear Reaction Data (EXFOR): Extended Computer Database and Web Retrieval System," NUCL. INSTRUM. METH. IN PHYS. RES. SEC. A **888**, 31–43 (2018).

[36] J.M. O'Donnell,"A New Method to Reduce the Statistical and Systematic Uncertainty of Chance Coincidence Backgrounds Measured with Waveform Digitizers," NUCL. INSTR. METHODS IN PHYS. RES. A **805**, 87–94 (2016).

[37] K.J. Kelly, T. Kawano, J.M. O'Donnell *et al.*, "Preequilibrium Asymmetries in the ^{239}Pu(n, f) Prompt Fission Neutron Spectrum," PHYS. REV. LETT. **122**, 072503 (2019).

[38] K.J. Kelly, M. Devlin, J.M. O'Donnell *et al.*, "Measurement of the ^{239}Pu(n,f) Prompt Fission Neutron Spectrum from 10 keV to 10 MeV Induced by 1–20 MeV Neutrons," PHYS. REV. C **102**, 034615 (2020).

[39] K.J. Kelly, J.A. Gomez, M. Devlin *et al.*, "Measurement of the ^{235}U(n,f) Prompt Fission Neutron Spectrum from 10 keV to 10 MeV Induced by Neutrons of Energy from 1 MeV to 20 MeV," PHYS. REV. C **105**, 044615 (2020).

[40] J.A. Gomez, J.M. O'Donnell, K.J. Kelly *et al.*, "Quantification of the Systematic Uncertainties Associated with Measuring a Chance Coincidence Background at Chi-Nu," Los Alamos National Laboratory Report LA-UR-19-20145 (2019).

[41] K.J. Kelly, M. Devlin, J.M. O'Donnell *et al.*, "Errors Introduced in Fission Neutron Spectrum Measurements using Single Reference," Nucl. Instrum. Meth. Phys. Res. A **1010**, 165552 (2021).

[42] B. Böttger, H. Klein, A. Chalupka *et al.*, "Investigation of the Spectral Fluence of Neutrons from Spontaneous Fission of ^{252}Cf by Means of Time-of-flight Spectrometry," Nucl. Sci. Eng. **106**, 377–398 (1990).

[43] H. Märten, D. Richter and D. Seeliger, "Analysis of Experimental Data on the High-energy End of the ^{252}Cf Spontaneous-fission Neutron Spectrum," IAEA Report INDC(GDR)-28L (1984).

[44] H. Märten, D. Richter, D. Seeliger *et al.*, "The ^{252}Cf Neutron Spectrum in the 5- to 20-MeV Energy Range," Nucl. Sci. Eng. **106**, 353–366 (1990).

[45] P. Staples, J.J. Egan, G.H.R. Kegel *et al.*, "Prompt Fission Neutron Energy Spectra Induced by Fast Neutrons," Nucl. Phys. **A591**, 41–60 (1995), EXFOR 13982.

[46] P. Marini, J. Taieb, B. Laurent *et al.*, "Prompt Fission Neutrons in the ^{239}Pu(n,f) Reaction," Phys. Rev. C **101**, 044614 (2020).

[47] D. Neudecker, "ARIADNE—A Program Estimating Covariances in Detail for Neutron Experiments," Europ. Phys. J. N **4**, 34 (2018).

[48] D. Neudecker, A.D. Carlson, S. Croft *et al.*, "Templates of Expected Measurement Uncertainties for Average Prompt and Total Fission Neutron Multiplicities," Europ. Phys. J. N same issue (2023).

[49] J. K. Dickens, "SCINFUL: A Monte Carlo Based Computer Program to Determine a Scintillator Full Energy Response to Neutron Detection for E_n between 0.1 and 80 MeV: User's Manual and FORTRAN Program Listing,"Oak Ridge National Laboratory Report ORNL-6462 (1988). Available online at *web.ornl.gov/info/reports/1988/3445605995426.pdf.* RSIC package number **PSR-267A**, last updated in 1989.

[50] K.J. Kelly, J.M. O'Donnell, J.A. Gomez *et al.*, "Numerical Integration of Detector Response Functions via Monte Carlo Simulations," Nucl. Instr. Methods in Phys. Res. A **866**, 182–189 (2017).

[51] A. Trkov and R. Capote, "Evaluation of the Prompt Fission Neutron Spectrum of Thermal Neutron-induced Fission of ^{235}U," Phys. Procedia **64**, 48–54 (2015).

[52] P. Talou, T. Kawano, D.G. Madland *et al.*, "Uncertainty Quantification of Prompt Fission Neutron Spectrum for n(0.5 MeV)+^{239}Pu," Nucl. Sci. Eng. **166**, 254–266 (2010).

[53] M.E. Rising, P. Talou, T. Kawano *et al.*, "Evaluation and Uncertainty Quantification of Prompt Fission Neutron Spectra of U and Pu Isotopes," Nucl. Sci. Eng. **175**, 81–93 (2013).

[54] F.-J. Hambsch, A. Tudora, G. Vladuca *et al.*, "Prompt Fission Neutron Spectrum Evaluation for ^{252}Cf(SF) in the Frame of the Multi-modal Fission Model," Ann. Nucl. Energy **32**, 1032–1046 (2005).

[55] OECD NEA Data Bank, JEFF-3.2 Evaluated Data Library—Neutron Data (2014), http://www.oecd-nea.org/dbforms/data/eva/evatapes/jeff_32/ (accessed on 8/11/2016).

[56] K. Shibata, O. Iwamoto, T. Nakagawa *et al.*, "JENDL-4.0: A New Library for Nuclear Science and Engineering," J. Nucl. Sci. Technol. **48**, 1–30 (2011).

[57] D.G. Madland and J.R. Nix, "New Calculation of Prompt Fission Neutron Spectra and Average Prompt Neutron Multiplicities," Nucl. Sci. Eng. **81**, 213–271 (1982).

[58] D.A. Brown, M.B. Chadwick, R. Capote *et al.*, "ENDF/B-VIII.0: The 8th Major Release of the Nuclear Reaction Data Library with CIELO-project Cross Sections, New Standards and Thermal Scattering Data," Nucl. Data Sheets **148**, 1–142 (2018).

[59] M.B. Chadwick, M. Herman, P. Oblŏzinský *et al.*, "ENDF/B-VII.1 Nuclear Data for Science and Technology: Cross Sections, Covariances, Fission Product Yields and Decay Data, " Nucl. Data Sheets **112**, 2887–2996 (2011).

[60] M.B. Chadwick, P. Oblŏzinský, M. Herman *et al.*, "ENDF/B-VII.0: Next Generation Evaluated Nuclear Data Library for Nuclear Science and Technology", Nucl. Data Sheets **107**, 2931–3060 (2006).

[61] B. Becker, P. Talou, T. Kawano *et al.*, "Monte Carlo Hauser-Feshbach Predictions of Prompt Fission γ Rays: Application to $n_{\rm th}$+^{235}U, $n_{\rm th}$+^{239}Pu, and ^{252}Cf (sf)," Phys. Rev. C **87**, 014617 (2013).

[62] O. Litaize and O. Serot, "Investigation of Phenomenological Models for the Monte Carlo Simulation of the Prompt Fission Neutron and γ Emission," Phys. Rev. C **82**, 054616 (2010).

[63] R. Vogt, J. Randrup, J. Pruet *et al.*, "Event-by-event Study of Prompt Neutrons from ^{239}Pu(n,f)," Phys. Rev. C **80**, 044611 (2009).

[64] H.Y. Lee, T.N. Taddeucci, R.C. Haight *et al.*, "Li-glass Detector Response Study with a ^{252}Cf Source for Low-energy Prompt Fission Neutrons," Nucl. Instr. Methods in Phys. Res. A **703**, 213–219 (2013).

[65] G. Knoll, *Radiation Detection and Measurement.* 3rd Edition, John Wiley and Sons Inc (2000).

[66] B. H. Armitage and M. G. Sowerby (Eds), in *Proc. of EURATOM Specialist Meeting on Inelastic scattering and Fission Neutron Spectra, AERE, Harwell, UK*, AERE Report **AERE-R-8636** (1977). See Appendix A with detailed corrections for past data sets.

[67] R.B. Leachman and L. Blumberg, "Fragment Anisotropies in Neutron-, Deuteron-, and Alpha-Particle-Induced Fission,"Phys. Rev. **137**, B814–B825 (1965).

[68] V.G. Nesterov, Yu.A. Blyumkina, L.A. Kamaeva *et al.*, "Angular Distribution of Fragments from Fission of ^{235}U and ^{239}Pu by 0.08–1.25 MeV Neutrons,"Atomnaya Energiya **16**, 519–521 (1964).

[69] J. E. Simmons and R. L. Henkel, "Angular Distribution of Fragments in Fission Induced by MeV Neutrons"Phys. Rev. **120**, 198–210 (1960).

[70] K.J. Kelly, J.A. Gomez, J.M. O'Donnell *et al.*, "Utilization of MCNP6 Implicit-capture Simulations for Quantification of Systematic Uncertainties from Experimental Environments," Nucl. Instr. Methods in Phys. Res. A **954**, 161411 (2020).

[71] C.J. Werner (ed.), "MCNP Users Manual - Code Version 6.2," Los Alamos National Laboratory Report LA-UR-17-29981 (2017).